

Contact SLAM: An Active Tactile Exploration Policy Based on Physical Reasoning Utilized in Robotic Fine Blind Manipulation Tasks

Gaozhao Wang, Xing Liu*, Zhenduo Ye, Zhengxiong Liu and Panfeng Huang

Abstract—Contact-rich manipulation is difficult for robots to execute and requires accurate perception of the environment. In some scenarios, vision is occluded. The robot can then no longer obtain real-time scene state information through visual feedback. This is called “blind manipulation”. In this manuscript, a novel physically-driven contact cognition method, called “Contact SLAM”, is proposed. It estimates the state of the environment and achieves manipulation using only tactile sensing and prior knowledge of the scene. To maximize exploration efficiency, this manuscript also designs an active exploration policy. The policy gradually reduces uncertainties in the manipulation scene. The experimental results demonstrated the effectiveness and accuracy of the proposed method in several contact-rich tasks, including the difficult and delicate socket assembly task and block-pushing task.

Index Terms—Force and Tactile Sensing, Perception for Contact-rich Manipulation, Active Tactile Exploration.

I. INTRODUCTION

In robotic manipulation tasks, vision plays an irreplaceable role. Through visual servoing, a robot can identify the target of manipulation and control its manipulator to complete the task [1]. In this process, the tactile or force sensing is mainly used to interact with the environment after the vision has already provided the target position [2].

However, in certain tasks, when vision fails or is occluded, the robot can no longer obtain real-time scene state information via visual feedback. We refer to such manipulation tasks as “blind manipulation” tasks, in which the robot must rely solely on tactile and force information. Compared with visual sensing, tactile sensing provides more comprehensive information about the contact state with the environment during manipulation, including the geometry of the contacted object [3], the contact force/torque and its distribution [4], and contact event triggering [5]. Some researches have tried to transform the force or tactile signals into some forms of contact state [6]–[8]. The manipulation based on contact states tends to focus on low-level state feedback and control, such as determining whether specific signals relevant to task completion are present during contact [9] or designing contact feedback control loops [10]–[12] to replicate particular contact signals, but these methods usually have strong data

Gaozhao Wang, Xing Liu(Corresponding author), Zhenduo Ye, Zhengxiong Liu and Panfeng Huang are with the Research Center for Intelligent Robotics, the National Key Laboratory of Aerospace Flight Dynamics, and Shaanxi Province Innovation Team of Intelligent Robotic Technology, School of Astronautics, Northwestern Polytechnical University, Xi'an 710072, China. (e-mail: gaozhao_wang@mail.nwpu.edu.cn.)

dependency, and the utilized scene is constrained strictly. With these perceptual features, they can be further applied to robotic manipulation tasks [13], [14]. In terms of interaction with the environment, end-to-end policy generation is typically implemented through a sim-to-real approach [15]. Although some studies have investigated the perception process during manipulation with tactile sensing, they typically stop at the perception stage without conducting an in-depth study on task completion. The detailed comparison between the visual and tactile servo control process is shown in Fig. 1

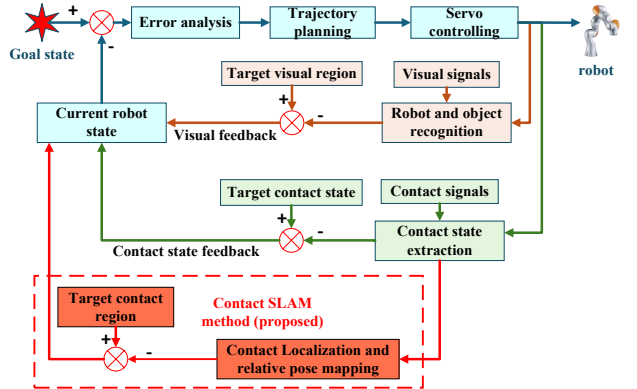


Fig. 1. The perception and cognition process in robot manipulation tasks. In general, the visual signals are used to understand the scene. When the vision is occluded, other kinds of information, such as tactile signals, are used to obtain contact states. However, the contact state is hard to be labelled and classified. We proposed the contact SLAM method, which doesn't pursue obtaining an exact contact state. Instead, it acquires the contact area with the environment through the cognitive process during the exploration of the environment.

During human manipulation, in addition to visual awareness of the process, there is also contact awareness. By judging the force sensed at the fingertips, people can estimate whether the manipulation goal has been reached and, if not, how far they are from the target state. This is a typical simultaneously localization and mapping(SLAM) problem. Sudharshan Suresh et al. [16] proposed using force–tactile sensing to simultaneously track an object's position and model its contour, a method they termed Tactile SLAM. Jialiang Zhao et al. [17] introduced the concept of FingerSLAM. Paloma Sodhi et al. [18] applied the SLAM modeling concept to object manipulation control, achieving tactile-based pushing operations. However, in blind manipulation tasks, except for the missed visual information, there also exists uncertainties, which could prevent the task to be finished, but the existing tactile methods don't consider

this.

In manipulation planning process, the uncertainty eliminating is widely used in the contact process [19], [20], but they usually use the binary force singal, and they often cosider one target object without interference from other objects. So Inspired by tactile SLAM methods and contact-driven blind manipulation methods, we introduce physically-driven contact cognition into robotic blind manipulation. By reasoning about the contact state between the grasped object and the environment from contact signals, the robot can continuously estimate and explore the environment until ultimately completing the manipulation task, as illustrated in Fig.1.

The contributions of this paper are as follows:

- 1) **A contact state-based pipeline for executing the contact-rich manipulation is proposed.** The contact-rich manipulation process is defined as the contact state translation process, and the relative pose between the grasped object and scene could be inferred from the contact state.
- 2) **A contact event-based SLAM method for environment perception and localization is proposed.** This method defines the contact event and further develops and extends the scope of tactile SLAM, proposing a post-estimation framework for relative pose estimation, enabling the perception and understanding of the scene state based on prior scene knowledge and contact event feedback.
- 3) **An effective planning method for fine blind manipulation based on active tactile exploration is proposed.** This approach balances environmental exploration with task completion efficiency, plans optimal action strategies according to the current understanding of the environment, and reduces the uncertainties of the manipulation scene gradually.

II. PROBLEM FORMULATION: CONTACT SLAM ANALYSIS

In blind manipulation tasks, several kinds of objects need to be noticed. The grasped objects, which are grasped by the gripper, and the tactile sensors could only perceive the tactile signals between the grasped objects and the gripper. The manipulated objects, which are used to interact with the grasped objects, including unmovable obstacles and movable objects. The last is the target region, which the grasped objects or manipulated objects need to reach. The detailed scenes are shown in section IV-A.

In order to represent the pose and of these things, the coordinates used in this manuscript are illustrated in Fig. 2(a), and the iteration between the grasped object and obstacles is shown in Fig. 2(b).

To achieve the task objectives, we make the following assumptions:

- 1) There exists a relative motion tendency between the grasped object and the gripper, but no relative translational displacement.
- 2) The contact between objects is quasi-static.
- 3) The precise geometric dimensions and shapes of the grasped object and the manipulated object are known in advance.

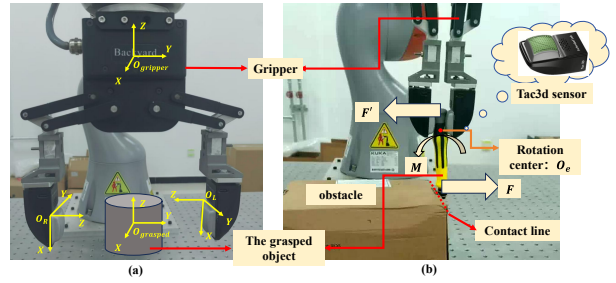


Fig. 2. (a) represents the coordinates used in this manuscript. The left and right sensor coordinates are opposite to the left and right positions in space because of sensor setting. (b) represents the corresponding forces and torques applied to the object when contact happens.

- 4) All objects in the environment are static and do not move autonomously; the only moving bodies are the gripper and the objects it holds.

Contact SLAM aims to address the problems of relative pose localization between objects and environment reconstruction in contact-rich manipulation tasks, and then plans the subsequent end-effector motion trajectory for the robot.

According to the definition of SLAM, contact SLAM also includes both localization and mapping components:

- **Localization** focuses on determining the positions of the robot end-effector, the grasped object, the target object, and other objects of interest in the environment.
- **Mapping** involves determining the positions of the landmarks in the environment by representing and analyzing the current contact information between the grasped object and the environment. This approach does not seek to obtain an accurate contact configuration of the grasped object within the environment; instead, it only requires relative contact-region information, which is sufficient to satisfy the manipulation task requirements.

The complete contact SLAM method includes tactile perception, localization, mapping and active exploration process, as illustrated in Fig. 3.

III. METHODS

A. Contact Force Estimation Analysis

The Tac3D sensor used in this study provides the three-dimensional force distribution, the resultant three-dimensional force, and the resultant three-dimensional torque in the sensor coordinate frame. These enable researchers to determine not only the magnitude but also the trend of forces acting on the grasped object.

When a two-finger gripper grasps an object, all forces acting on the grasped object are reflected in the tactile sensors mounted on the gripper fingers. The two-finger gripper and the grasped object could be modeled as a beam fixed at one end. When an external force is applied to one end, the reaction at the gripper includes not only a force in the opposite direction but also a torque relative to the grasping point. Both the forces and torques are applied to the tactile sensors mounted on the gripper.

As illustrated in Fig. 2(b), when a force in a certain direction acts on the grasped object, it could be decomposed into three

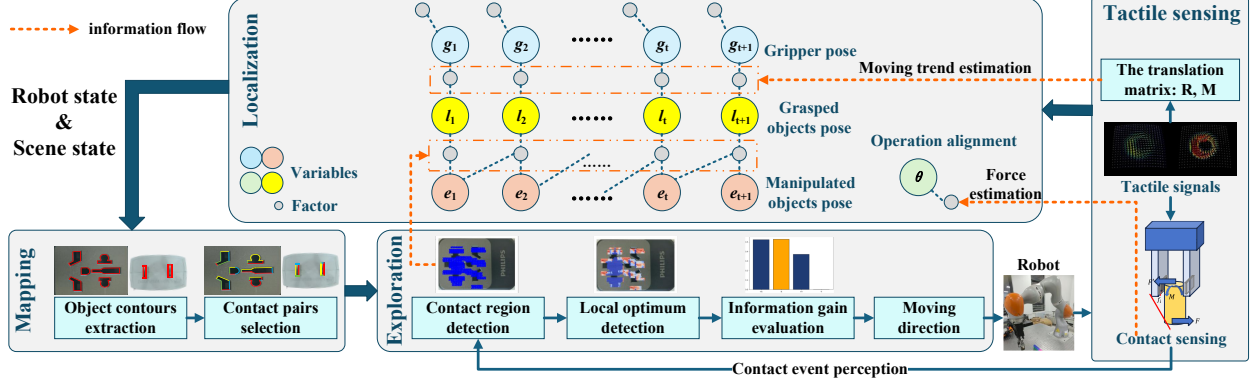


Fig. 3. The complete process of the proposed method. The method regards the manipulation process as an SLAM problem. In the localization phase, it focuses on determining the positions of the robot end-effector, the grasped object, and other objects of interest in the environment. In the mapping phase, it focuses on representing the current relative contact information together with the tactile information between the grasped object and the environment. After one SLAM process, generate the action strategy based on the information gain evaluation in different movement directions, then the robot executes the strategy, the tactile sensing converts the tactile signals into physical information and sends them to the SLAM process.

components along the X , Y , and Z axes of the gripper coordinate system. To maintain the stability of the grasped object, the two gripper fingers produce corresponding torques on the object. The relationship between the forces applied to the object and those measured by the gripper tactile sensors can be expressed as follows:

$$\begin{cases} F_x = F_y^R - F_y^L \\ F_y = F_z^L - F_z^R \\ F_z = F_x^L - F_x^R \end{cases} \quad (1)$$

where F_x , F_y , and F_z are force components in the frame of the gripper. F_i^L and F_i^R are corresponding force components ($i = x, y, z$) in the frame of the left sensor and right sensor.

B. State Perception and Optimization

We employ factor graph optimization as our estimation framework, which is based on the principle of maximum a posteriori (MAP) estimation. A factor graph is a bipartite graph with two types of parameters: variables x and factors ϕ . Variable nodes are the latent states to be estimated, and factor nodes encode constraints on the variables, such as measurement likelihood functions, or physics, geometric models [18]. Under Gaussian noise model assumptions, MAP inference is equivalent to solving a nonlinear least-squares problem. That is, for Gaussian factors $\phi_i(x)$ corrupted by zero-mean, normally distributed noise, the inference equation is:

$$\hat{x} = \operatorname{argmin}_x \frac{1}{2} \sum_{i=1}^n \|F_i(x)\|_{\sum_i}^2 \quad (2)$$

In contact SLAM, following factors are optimized:

- **Gripper Localization Factor F_{gri} :** The position of the gripper g_t can be derived from the position of the robot's end-effector

$$\|F_{gri}(g_t)\|_{\sum_{gri}}^2 = \|g_t - g_t^{pri}\|_{\sum_{gri}}^2 \quad (3)$$

- **Grasped object Localization Factor F_{obj} :** The position of the object grasped by the gripper l_t can be obtained from the gripper position and the relative displacement

of the object sensed by the tactile sensor mounted on the gripper. Based on the prior method [21], we define several coordinate frames: the gripper coordinate frame $(OXYZ)_g$, sensor coordinate frame $(OXYZ)_s$, grasped object coordinate frame $(OXYZ)_o$, and world coordinate frame $(OXYZ)_w$. Our estimation target is the position of a grasped object in the world coordinate frame, and the factor expression is:

$$\|F_{obj}(l_t, g_t)\|_{\sum_{obj}}^2 = \|l_t - T_g^w T_s^g T_l^s I\|_{\sum_{obj}}^2 \quad (4)$$

here, T_g^w represents the gripper pose which could be derived from the robot's end-effector pose, T_s^g is fixed during operation, and T_l^s depends on the relative displacement of the marker points sensed by the tactile sensor, which could be decomposed as: $T_l^s = T_{sd}^s T_l^{sd}$, where T_l^{sd} is unchanged. To obtain T_{sd}^s , the SVD-based optimization process is acquired:

$$R^*, M^* = \min_{R, M} \sum_{i=1}^N \|p_i - (R \cdot p'_i + M)\|^2 \quad (5)$$

where the translation matrix T_{sd}^s is composed of the optimized rotation matrix R^* and translation matrix M^* .

- **Environment Localization Factor F_{env} :** Based on the contact pairs obtained through active exploration and the object position at time t , the position of obstacles e_t can be estimated. The estimated pose of environment in $(OXYZ)_w$ is:

$$\|F_{env}(e_t, e_{t-1}, l_t)\|_{\sum_{env}}^2 = \|B(l_t + B(P_t)) \cup B(l_t - B(P_t)) \cap e_{t-1} - e_t\|_{\sum_{env}}^2 \quad (6)$$

where $B(\cdot)$ means the boundary of the objects or obstacles' position. The parameter P_t is the distribution range of particles at the current time, which is shown in section III-C. Initially, the e_0 is set to a range that could cover the potential position of interested objects.

- **Operation Alignment Factor F_{ali} :** During manipulation, researchers are not concerned with the absolute position of the object being manipulated; rather, they focus on

whether the correct contact state has been achieved. Therefore, we define the following operation alignment factor:

$$\|F_{ali}(\theta_{ali})\|_{\sum_{ali}}^2 = \|E(F_x \cap F_y \cap d) - \theta_{ali}\|_{\sum_{ali}}^2 \quad (7)$$

where F_x, F_y are force components calculated by equation 1, and d represents the distance. $E(\cdot)$ represents a function used for measuring the error between the current state and the goal state. θ_{ali} is a binary independent variable, if $\theta_{ali} = 1$, the task is considered to be finished.

C. Contact Localization and Active Tactile Exploration Policy

In the process of blind manipulation, the exact pose of the object is unknown. To achieve the goal of estimating relative contact regions, the system must generate exploratory actions to interact with the environment, continuously estimate the contact state during the contact process, and adjust the action based on the tactile sensor feedback. Based on these, we draw inspiration from active localization methods [22] and propose the **Contact Localization and Active Tactile Exploration Policy** method. The detailed workflow is shown as follows:

Preparation stage: At this stage, given that the exact geometric shapes of the objects in the environment and the grasped object are all represented as polygons, and their vertices v_1, v_2, \dots, v_N are collected in counterclockwise order. The contour edges can then be computed as: $e_i = v_{i+1} - v_i$, and the outward normal vector of each contour edge is given by: $n_i = (e_i^y, -e_i^x)$. Thus, we can define the contour of the grasped object and contours of other objects in the environment: $S_{e_i} = \{(n_i, v_i, v_{i+1}) | i = 1, \dots, N_i\}$, $S_{l_j} = \{(n_j, v_j, v_{j+1}) | j = 1, \dots, M_j\}$. And $C_{env} = \{S_{e_1}, S_{e_2}, \dots, S_{e_N}\}$, $C_{object} = \{S_{l_1}, S_{l_2}, \dots, S_{l_M}\}$.

After that, to represent the relative position state between the grasped object and the scene objects, the distribution of the reference point within the environment is initialized. In the manuscript, we choose the particle filtering method. The distribution of particles at time t is represented as P_t , and the weight of each particle is represented as $w_i^t = 1/\text{len}(P_t)$.

Step 1, Local optimum detection. Examine the weights and choose the local optimum as follows: $\text{peaks} = \{p_i^t | p_i^t \in P_t, w_i^t > 0.5/\text{len}(P_t), i = 1, 2, \dots, n\}$. If the boundary measurement of peaks within δ_{thr} , the distribution of peaks is taken as the potential region of the reference point. If not, the process turns to Step 2 to select a movement direction.

Step 2, Information gain evaluation: For each potential motion direction of the object, the expected information gain is calculated, which is represented as the types of contact states of motion distance. We choose the entropy as the justance criterion, and calculate the entropy of each action as follows:

$$\text{entropy}(Z_a) = \sum_{z \in Z_a} -p(z) \log p(z) \quad (8)$$

Where Z_a is the predicted contact state set of all particles with the action a .

Afer getting the information gain of each potential action, we choose the action which could get the most information as the moving direction: $\max_a \{\text{entropy}(Z_a)\}$.

Step 3, Exploration through motion: The grasped object moved in the selected direction until a change in the tactile signal is detected.

Step 4, Contact pair selection and updation of particles:

After detecting a tactile signal change, we can estimate the direction of the force acting on the grasped object. From the perspective of object dynamics, the force direction and the outward normal vector of the object's contour satisfy the following relationship: $F_G^t \cap n_i > 0, F_G^t \cap n_j < 0$. Thus, the contact pairs can be represented as: $(i, j) = \{n_i = -n_j\}$, and the distribution of particels is updated as follows: $P_t = P_{t-1} \cap (B(S_{e_i}) \cup B(S_{l_j}))$.

Step 5, Particles' weights updation: After selecting the candidate contact pairs, we then backtrack the contact events during the motion trajectory. Specifically, based on the traveled distance $Distance$ and the number of motion steps T , we infer the potential contact states at intermediate time steps. If at any of these time steps, the inferred contact state is inconsistent with the observed tactile signal, the weight of the corresponding particle is reduced. This process is repeated until the weights of all particles are updated. The weight w_i^t is updated as follows:

$$w_i^{t+1} = w_i^t \cdot \mathcal{P}(z_{obs}^t, z_{pred}(p_i - (T - t)/T \cdot Distance)) \quad (9)$$

where z_{obs}^t represents the tactile obserbation at the t time, z_{pred} represents the predicted tactile signal at the pose of $p_i - (T - t)/T \cdot Distance$.

After updating the weights of particles, the local optimum detection process is repeated, and the particles are further updated: $P_t = \text{peaks}$.

If particles' distribution is less than the predefined threshold, the process turns to Step 7 to find the optical policy to finish the task. If not, the process turns to Step 6 to resample more particles.

Step 6, Resample particles: After updating the weights of all particles, we check the number of particles. If the number of particles is less than a predefined threshold (e.g., 50), we resample additional particles within the current potential region to ensure sufficient particle density for accurate localization. Based on the particle filter method, we choose to resample the same number of particles each iteration.

Return to the Step 1 and continue the exploration process.

Step 7, The generation of final manipulation policy:

When the particles' distribution is smaller than the set threshold, the manipulation policy is generated. The optimal policy is represented as moving from the estimated object pose to the target pose. In the motion planning process, we choose the A_star algorithm as the planning method.

D. The improved tips of Active Exploration

In order to improve the efficiency of the active exploration, we adopt the following improvements:

First, the distance variance criterion is added to the process of calculating the information gain. When the distribution of particles is small, the entropy calculation could become very small, too. That means the information gain is useless in the choice of action direction. When the entropy calculation is

small, the distance variance is added to the information gain. A larger distance criterion value indicates greater variability in the motion of the current particle distribution, enabling more particles to be distinguished based on the discrepancy between the estimated motion distance and the actual motion distance.

The details of Gain information calculation is shown in Algorithm 1.

Algorithm 1: Information Gain Evaluation

Input:

- 1: The potential distribution of movable objects:
 $P_t = peaks;$
- 2: The reference actions: $A = \{a_1, a_2, \dots, a_m\};$
- 3: The contour of environment: $C_{env} = \{S_{e_1}, S_{e_2}, \dots, S_{e_N}\};$
- 4: The contour of grasped object:
 $C_{object} = \{S_{l_1}, S_{l_2}, \dots, S_{l_M}\};$

Output:

- 5: **if** $len(P_t) = 1$: **then**
- 6: Choose the optimal trajectory;
- 7: **end if**
- 8: **if** $len(P_t) > 1$: **then**
- 9: **for** $a \in A$ **do**
- 10: **for** $p \in P_t$ **do**
- 11: Calculate the contact state: z_pred at p with action a ;
- 12: Add z_pred to Z_a ;
- 13: Calculate the distance d to get the state z_pred ;
- 14: Add d to D_a ;
- 15: **end for**
- 16: Calculate the entropy of Z_a :
 $entropy(Z_a) = \sum_{z \in Z_a} -p(z) \log p(z);$
- 17: Calculate the variance of D_a :
 $var(D_a) = \sum_{d \in D_a} (d - \mu(D_a))^2;$
- 18: **end for**
- 19: **if** $\max\{entropy(Z_a)\} < e_{thr}$: **then**
- 20: Choose the action based on the Distance variance:
 $\max_a\{var(D_a)\};$
- 21: **else**
- 22: Choose the action which could get the most information: $\max_a\{entropy(Z_a)\}.$
- 23: **end if**
- 24: **end if**

Second, we adjust the number of particles to resample. Instead of resampling the same particles in each episode. In environments with imperfect or imprecise modeling, overly rapid particle depletion may cause some plausible distribution regions to be discarded prematurely. A straightforward solution is to increase the number of particles during resampling. However, if the resampled particle count is fixed, an insufficient number of particles fails to improve localization accuracy, while an excessive number leads to particle over-crowding in later iterations, or even to a continuous increase in the total particle count during the filtering process. To balance exploration efficiency and localization accuracy, we therefore design an adaptive particle resampling mechanism. This mechanism maintains a reasonable particle density in

all potentially valid distribution regions, thereby reducing the probability that correct hypotheses are eliminated due to incidental or unexpected events.

The whole **Active Tactile Exploration policy** is shown in Algorithm 2.

Algorithm 2: Active Tactile Exploration Policy

Preparation:

- 1: Scene construction and obtain $C_{env}, C_{object};$
- 2: Initialization of the reference point distribution:
 $P_t = \{p_1, p_2, \dots, p_n\}, W_t = \{w_1^t, w_2^t, \dots, w_n^t\};$

Output:

- 3: Local optimum detection: $P_t = peaks = \{p_i^t | p_i^t \in P_t, w_i^t > 1/\text{len}(P_t), i = 1, 2, \dots, n\};$
- 4: Information gain evaluation and obtain action $\pi;$
- 5: Execute π and monitor force until the contact occurs;
- 6: Updation of particles: $P_{t+1} = P_t \cap (B(S_{e_i}) \cup B(S_{l_j}));$
- 7: Update the particles' weights:
 $w_i^{t+1} = w_i^t \cdot \mathcal{P}(z_{obs}^t, z_{pred}(p_i - (T - t)/T \cdot Distance)),$
 $W_{t+1} = w_i^{t+1} | i = 1, 2, \dots, \text{len}(P_{t+1});$
- 8: Resample particles: $P'_{t+1} = AR(P_{t+1}, P_t, W_{t+1})$
- 9: **if** $B(peaks) > \delta_{thr}$ **then**
- 10: return to “Local optimum detection”.
- 11: **else**
- 12: Find the optimal trajectory $\pi;$
- 13: Execute π , until the alignment factor satisfies $\theta_{ali} = 1;$
- 14: **end if**

IV. EXPERIMENTAL STUDIES

A. Experimental Setup

This manuscript defines two blind manipulation task scenarios, which are illustrated in Fig. 4.

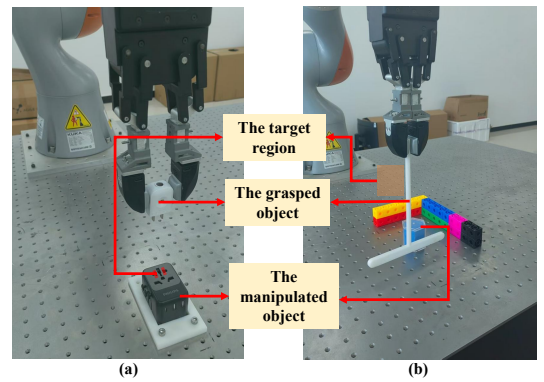


Fig. 4. The calibration task scenario and two manipulation experiment scenarios. (a) represents the calibration process of the Tac3D sensor; (b) represents the socket assembly task scenario; (c) represents the block-pushing task scenario.

The first task scenario involves a blind peg-in-hole assembly of a power socket component of two different standards. The robot is required to grasp the socket and insert it into the correct receptacle. The second task scenario is a blind pushing task in the presence of obstacles. In this scenario, the operator has prior knowledge of the approximate position of the block

to be pushed, the target location, as well as the geometrical shapes of the obstacles present in the environment. However, the exact positions of these obstacles within the scene are unknown. The chosen two tasks are all typical blind indirect contact manipulation tasks, because the contact with the scene needs to be referred from the contact signals between the gripper and the grasped object.

- **Evaluation metrics:** After the mapping process, we calculate the localization error represented as root mean square error(RMSE) and iteration times. After the manipulation process, we evaluate the whole exploration time of manipulation, as well as the success rate.
- **Compared methods:** We choose the **Spiral-hole-searching** method, which is a typical passive searching method, as the baseline and control method.

B. Results of the Socket Assembly Experiments

In this experiment, we used two different plugs: a two-pin plug and a triangular three-pin plug, to assemble into the same socket, as illustrated in Fig. 4(b). The main challenge of this task lies in the need to distinguish between different assembly regions corresponding to different plug geometries. In the absence of visual guidance, the robot must rely solely on tactile feedback and prior knowledge of the scene to identify and reason about the relative contact regions between the plug and the socket.

1) *The ablation experiments:* We introduce two improvements to the particle filtering procedure, namely a distance variance criterion and adaptive resampling. The necessity of these improvements is demonstrated through ablation experiments. Specifically, for each type of socket pin, we select a random initial pose, and conduct the control group(fixed resampling without the distance variance criterion) and two experimental groups, one using the distance criterion alone and the other combining the distance criterion with adaptive resampling.

For the control group, since entropy is the only information criterion, when the particle distribution becomes highly concentrated, the resulting motion direction is unique in all cases, as shown in Fig. 5. This indicates that the entropy criterion fails under such conditions. To address this issue, we introduce the **distance variance criterion** as shown in Section III-D. The specific implementation is as follows: when all entropy values fall below 10^{-2} , the decision criterion is switched from entropy to the distance criterion. We then reattempt exploration in the previously failed scenarios. As shown in Fig. 5, the results demonstrate that, after introducing the distance criterion, effective environment exploration can still be achieved even when the entropy criterion is extremely small, thereby leading to correct localization results.

In the control group, a resampling strategy was adopted in which resampling is triggered only when the number of particles falls below 50. Under this strategy, accumulated particle position errors in earlier stages may result in certain particle modes being eliminated from the new particle set before the resampling threshold is reached, as illustrated in Fig. 6, ultimately causing localization failure. We added the

adaptive resampling to the filter process as shown in Section III-D, and the rule of resampling is as follows:

$$scale = \begin{cases} \frac{P_t}{3 \times P_{t+1}} & len(P_{t+1}) > 300 \\ \frac{P_t}{2 \times P_{t+1}} & 100 \leq len(P_{t+1}) \leq 300 \\ \frac{P_t}{P_{t+1}} & 50 \leq len(P_{t+1}) < 100 \\ \frac{2 \times P_t}{P_{t+1}} & len(P_{t+1}) < 50 \end{cases} \quad (10)$$

$$P'_{t+1} = scale \times P_{t+1} \quad (11)$$

The results are shown in Fig. 6. It can be observed that, after incorporating adaptive resampling, the particle distribution was better maintained, and the localization process successfully converged to a unimodal distribution.

2) *The comparative experiments:* To verify the accuracy of the proposed method for estimating the relative position of the peg and the hole, we conducted 25 sets of experiments for each pin assembly task. The initial position of each set of experiments was randomly selected within the plane of the hole. In total, 50 sets of experiments were carried out for data analysis. For the control group, we also conducted 25 sets of experiments for each pin at arbitrary initial positions, making a total of 50 sets of experiments for comparison. For the experimental group, when the estimation of the relative position between the plug and the socket converges to a unimodal distribution, we use the method as described in the article [23] for the final assembly operation. For the spiral hole-searching method used for comparison, we set the following threshold conditions: $F_{x/y} > 0.55 * F_z$ if $F_z > 0.5$; $F_{x/y} > 0.9$ if $F_z < 0.5$. If the threshold conditions are met, it is considered that the hole area has been found, and then the plug is inserted downward and it is checked whether the assembly is completed. For both the experimental group and the control group, the conditions for successful assembly are: $d_z > 0.025$ and $F_{x/y} > 0.9N$.

TABLE I
THE RESULTS OF SOCKET ASSEMBLY EXPERIMENTS.

	RMSE	Iter.Num	Explor.time	SR
two-pin	0.449mm	7.70	507.31s	80%
three-pin	0.698mm	9.95	679.96s	84%
sprial search	—	—	165.04s	10%

The experimental results are shown in Tab. I. It can be seen that the success rate of assembly using the contact positioning and active exploration tactile method is significantly higher than that of the control group. For the assembly tasks of the two types of bolts we selected, the success rates reached 80% and 84% respectively. In contrast, the spiral hole-searching method used for comparison only succeeded once in all attempts. This indicates that compared with the passive hole-searching method, the hole-searching method with active reasoning ability has significant advantages when facing an environment with redundancy and interference. The hole-searching method with active reasoning ability can model the environmental uncertainty, determine the possible potential positions, and then further narrow down the possible potential positions during continuous interaction, gradually eliminating

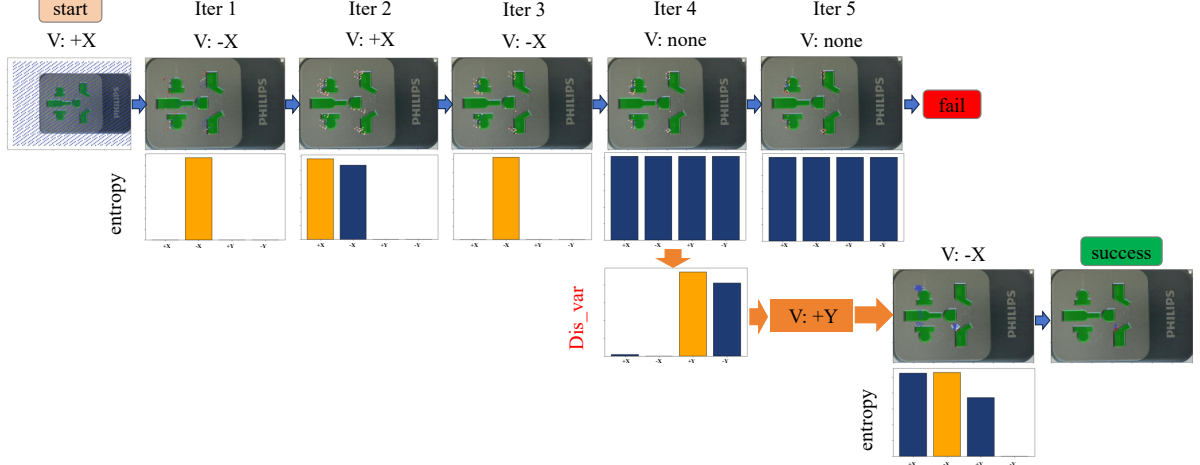


Fig. 5. The comparison of the control group and experimental group adding the distance criterion. In iteration 4, the entropy criterion is small and unique in all directions, indicating that the active exploration failed. After introducing the distance criterion, the optimal information gain is obtained.

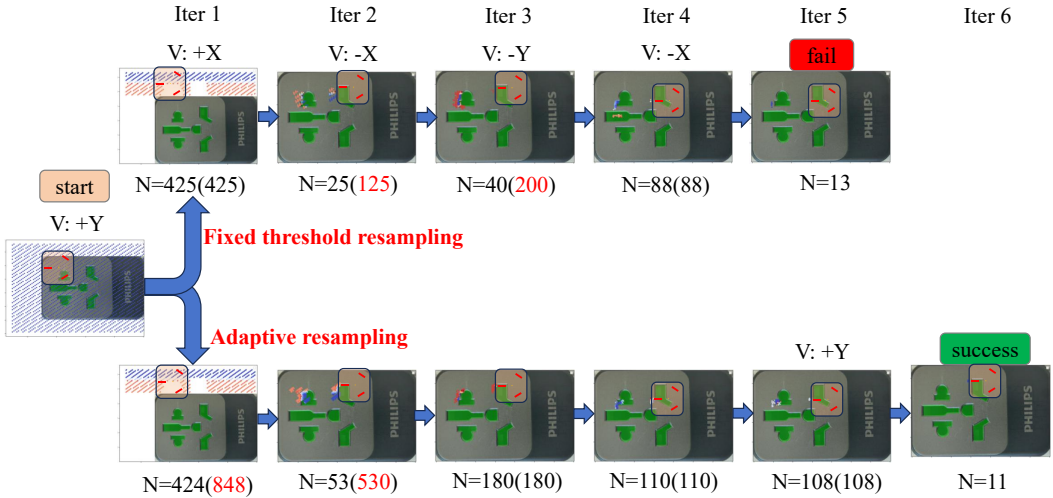


Fig. 6. The comparison of the control group and experimental group utilizes adaptive resampling. In iteration 5, the particle set around the plug was eliminated because of the accumulated position errors during exploration. In the experimental group,

the uncertainty. On the other hand, the passive search method is only suitable for situations with small errors. When there are large errors and environmental interference, due to the limitations of observation, it is likely to miss the correct position and fall into local optima.

Fig. 7 intuitively shows the process of relative position positioning using contact-based positioning and active tactile exploration. It can be seen that when the edge of the plug collides with the edge of the hole or goes beyond the hole area, the positions and weights of the particles are redistributed. Particles with too low weights or outside the potential distribution area are deleted. After 7 ~ 9 explorations, the distribution of the particles gradually stabilizes. If there is a single-peak distribution at this time, it indicates that the exploration is successful. Failed cases are mainly concentrated in situations where the active exploration fails to converge, that is, there is still a multi-peak distribution after the maximum number of exploration steps. The reason for the non-convergence of the

exploration is that the hole area is complex and the sizes of different areas are similar. If the plug falls into a hole area with a similar size, the exploration movement range will be greatly limited. If the plug has not explored the overall environmental area comprehensively at this time, the particles will remain in the hole areas with similar sizes and cannot converge to a single-peak distribution.

To verify the accuracy of the position localization results of contact SLAM, we verified the position estimation results of the socket obtained during the active exploration process. The results are shown in Fig. 8.

The reason why we chose to estimate the socket position in the environment as a verification of the positioning accuracy of contact SLAM is that during the task execution process, the positions of the gripper and the grasped object are constantly changing, and only the environment remains unchanged. As can be seen from Fig. 8, with the convergence of the particle distribution, the results of socket position estimation starting

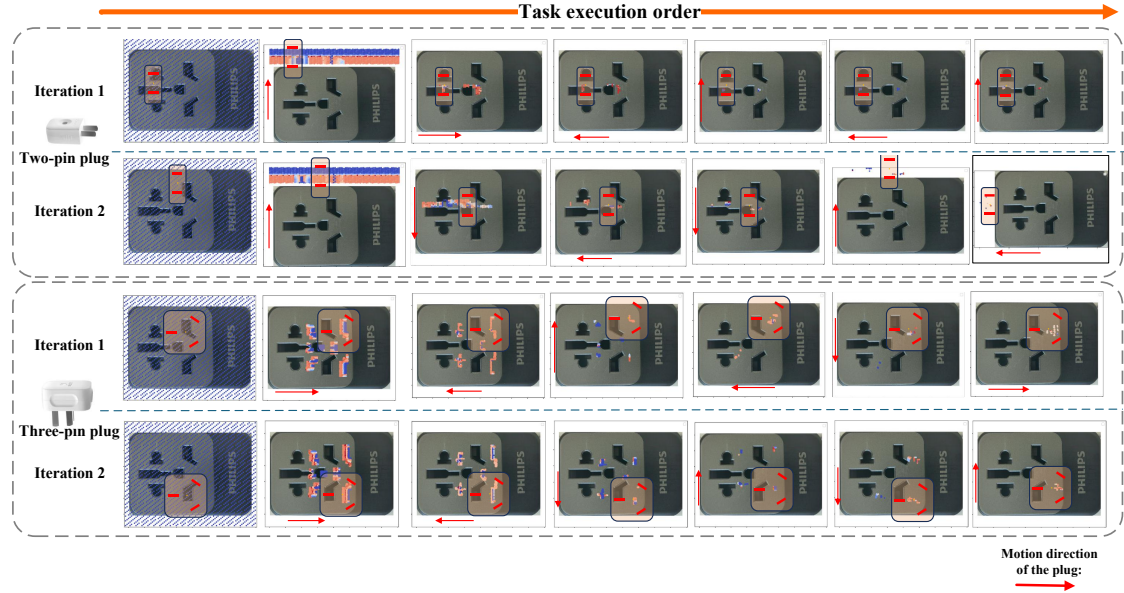


Fig. 7. The results of socket assembly experiments in different initial locations. The distribution of particles represents the potential relative pose of the plug and the socket. Red particles represent that the plug could be located at this point with more possibility, while the blue particles represent the less possibility.

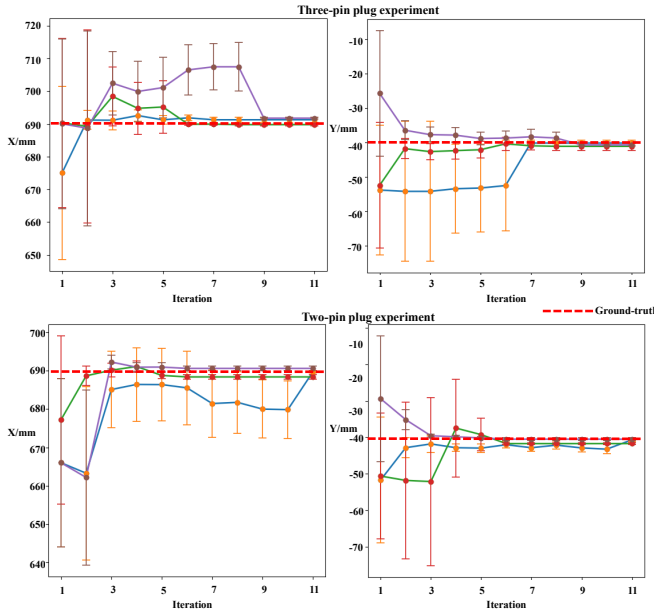


Fig. 8. The estimation results of the socket. Different initial position of gripper and plug got the same pose estimation of socket after several iterations.

from different initial positions will converge to the vicinity of the true value after exploration, and the error is within 2 mm, indicating the effectiveness of our contact SLAM for unknown estimation.

C. Results of the Blind Pushing Experiments

In this task, the robot must first detect the contact region between the block and the T-shaped tool. When obstacles are encountered, the robot estimates their relative positions, replans the task trajectory accordingly, and ultimately pushes

the block into the designated target region. The experimental results are illustrated in Fig. 9.

As shown in Fig. 9, in this task scenario, when obstacles are encountered, the robot is able to reduce the localization error of the obstacles to within 10 mm through a limited number of active explorations and contact interactions, which is sufficient to meet the requirements of trajectory re-planning.

D. Experimental Results Discussion

In the socket assembly experiment scenario, the success of perception depends on the complexity of the contact between the plug and the socket. For a two-pin plug, there are two planes in contact with the socket plane. Although the geometric shape of a three-pin plug is more complex, the part in contact with the socket plane is only its longest prong. Therefore, the contact situation of the two-pin plug is more complex, which also affects the number of exploration attempts. The number of exploration attempts for the two-pin plug is higher than that for the three-pin plug.

In the blind block-pushing experiment, it is crucial to distinguish between the movable block and the immovable obstacles. When an obstacle is encountered, the analysis of the particle distribution must take into account the size of the movable block. Compared with the case where the grasped object is in direct contact with the obstacle, the resulting particle distribution exhibits a translation shift.

V. CONCLUSION

This manuscript proposed a novel framework named contact SLAM, which could be utilized for fine blind manipulation tasks. The framework integrates tactile perception and physical reasoning to enable scene understanding and motion planning. Given prior knowledge of the objects' geometrical shapes and

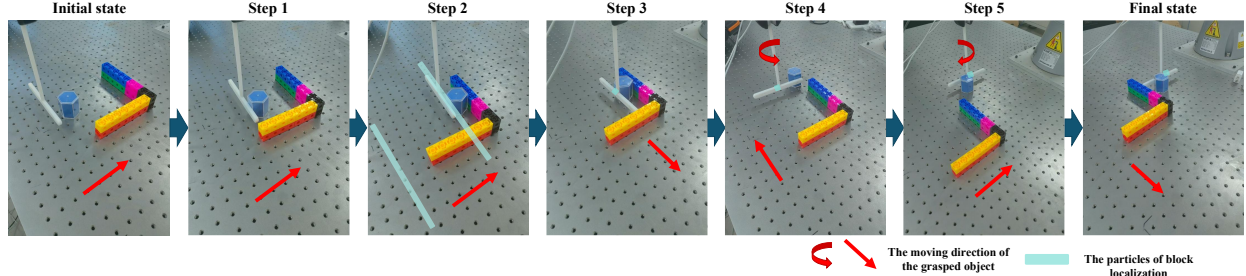


Fig. 9. The detailed results of the block-pushing task. The particle distribution represents the potential position ranges of the block and the obstacles.

dimensions, it allows the robot to precisely localize the relative pose between the grasped object and the manipulated object solely through tactile sensing, thereby accomplishing manipulation tasks without relying on visual information. The authors validated the effectiveness of the proposed framework through experiments on peg-in-hole assembly and block-pushing tasks. The present study primarily focuses on geometric constraints. In future work, the authors plan to extend this approach to incorporate dynamic constraints in fine manipulation, aiming to further enhance the robot's capability in executing such tasks.

REFERENCES

- [1] J. Marcos Correia Marques, N. Dengler, T. Zaenker, J. Mucke, S. Wang, M. Bennewitz, and K. Hauser, “Map space belief prediction for manipulation-enhanced mapping,” *arXiv e-prints*, pp. arXiv–2502, 2025.
- [2] C. Zhang, P. Hao, X. Cao, X. Hao, S. Cui, and S. Wang, “Vtla: Vision-tactile-language-action model with preference learning for insertion manipulation,” *arXiv preprint arXiv:2505.09577*, 2025.
- [3] J. Xu, H. Lin, S. Song, and M. Ciocarlie, “Tandem3d: Active tactile exploration for 3d object recognition,” in *2023 IEEE International Conference on Robotics and Automation (ICRA)*. IEEE, 2023, pp. 10 401–10 407.
- [4] Y. Zhang, Z. Kan, Y. Yang, Y. A. Tse, and M. Y. Wang, “Effective estimation of contact force and torque for vision-based tactile sensors with helmholtz–hodge decomposition,” *IEEE Robotics and Automation Letters*, vol. 4, no. 4, pp. 4094–4101, 2019.
- [5] K.-T. Yu and A. Rodriguez, “Realtime state estimation with tactile and visual sensing. application to planar manipulation,” in *2018 IEEE International Conference on Robotics and Automation (ICRA)*. IEEE, 2018, pp. 7778–7785.
- [6] T. Migimatsu, W. Lian, J. Bohg, and S. Schaal, “Symbolic state estimation with predicates for contact-rich manipulation tasks,” in *2022 International Conference on Robotics and Automation (ICRA)*. IEEE, 2022, pp. 1702–1709.
- [7] J. Lee and N. Fazeli, “Vitascope: Visuo-tactile implicit representation for in-hand pose and extrinsic contact estimation,” *arXiv preprint arXiv:2506.12239*, 2025.
- [8] S. Cao and J. Xiao, “On efficient and flexible autonomous robotic insertion assembly in the presence of uncertainty,” *IEEE Robotics and Automation Letters*, vol. 9, no. 7, pp. 6360–6367, 2024.
- [9] M. Noseworthy, B. Tang, B. Wen, A. Handa, C. Kessens, N. Roy, D. Fox, F. Ramos, Y. Narang, and I. Akinola, “Forge: Force-guided exploration for robust contact-rich manipulation under uncertainty,” *IEEE Robotics and Automation Letters*, 2025.
- [10] J. Bi, K. Y. Ma, C. Hao, M. Z. Shou, and H. Soh, “Vla-touch: Enhancing vision-language-action models with dual-level tactile feedback,” *arXiv preprint arXiv:2507.17294*, 2025.
- [11] H. Xue, J. Ren, W. Chen, G. Zhang, Y. Fang, G. Gu, H. Xu, and C. Lu, “Reactive diffusion policy: Slow-fast visual-tactile policy learning for contact-rich manipulation,” *arXiv preprint arXiv:2503.02881*, 2025.
- [12] A. Dutta, E. Burdet, and M. Kaboli, “Push to know!-visuo-tactile based active object parameter inference with dual differentiable filtering,” in *2023 IEEE/RSJ International Conference on Intelligent Robots and Systems (IROS)*. IEEE, 2023, pp. 3137–3144.
- [13] M. Bauza, A. Bronars, and A. Rodriguez, “Tac2pose: Tactile object pose estimation from the first touch,” *The International Journal of Robotics Research*, vol. 42, no. 13, pp. 1185–1209, 2023.
- [14] Y. Zhao, X. Jing, K. Qian, D. F. Gomes, and S. Luo, “Skill generalization of tubular object manipulation with tactile sensing and sim2real learning,” *Robotics and Autonomous Systems*, vol. 160, p. 104321, 2023.
- [15] M. Bauza, A. Bronars, Y. Hou, I. Taylor, N. Chavan-Dafle, and A. Rodriguez, “Simple, a visuotactile method learned in simulation to precisely pick, localize, regrasp, and place objects,” *Science Robotics*, vol. 9, no. 91, p. eadi8808, 2024.
- [16] S. Suresh, M. Bauza, K.-T. Yu, J. G. Mangelson, A. Rodriguez, and M. Kaess, “Tactile slam: Real-time inference of shape and pose from planar pushing,” in *2021 IEEE international conference on robotics and automation (ICRA)*. IEEE, 2021, pp. 11 322–11 328.
- [17] J. Zhao, M. Bauza, and E. H. Adelson, “Fingerslam: Closed-loop unknown object localization and reconstruction from visuo-tactile feedback,” *arXiv preprint arXiv:2303.07997*, 2023.
- [18] P. Sodhi, M. Kaess, M. Mukadam, and S. Anderson, “Learning tactile models for factor graph-based estimation,” in *2021 IEEE International Conference on Robotics and Automation (ICRA)*. IEEE, 2021, pp. 13 686–13 692.
- [19] M. S. Saleem, L. Yuan, and M. Likhachev, “A contact-driven framework for manipulating in the blind,” *arXiv preprint arXiv:2510.20177*, 2025.
- [20] M. S. Saleem, R. Veerapaneni, and M. Likhachev, “A pomdp-based hierarchical planning framework for manipulation under pose uncertainty,” *arXiv preprint arXiv:2409.18775*, 2024.
- [21] D. Ma, S. Dong, and A. Rodriguez, “Extrinsic contact sensing with relative-motion tracking from distributed tactile measurements,” in *2021 IEEE International Conference on Robotics and Automation (ICRA)*, 2021, pp. 11 262–11 268.
- [22] S. Agarwal, A. Tamjidi, and S. Chakravorty, “Motion planning in non-gaussian belief spaces (m3p): The case of a kidnapped robot,” *arXiv preprint arXiv:1506.01780*, 2015.
- [23] A. S. Morgan, Q. Bateux, M. Hao, and A. M. Dollar, “Towards generalized robot assembly through compliance-enabled contact formations,” *arXiv preprint arXiv:2303.05565*, 2023.